Analysis of the Charge Collection Mechanism of the Diamond Based on a Multi-physics Method

Yong Li [1,2*], Haiyan Xie [2], Linyue Liu [2], and Jianfu Zhang [2]

[1] School of Electronic and Information Engineering
Xi'an Jiaotong University, Xi'an 710049, China
liyong@mail.nint.ac.cn

[2] Northwest Institute of Nuclear Technology
Xi'an, 710024, China
xiehaiyan@nint.ac.cn, liulinyue@nint.ac.cn, zhangjianfu@nint.ac.cn

Abstract **—** Diamond is one of the most important wide-band-gap semiconductors for radiation detection and electronic device upgrading, however, for the lack of effective quantitative simulation method, the generation, recombination and movement of carriers in this material are still far from fully studied. In this paper, a multi-physics method for quantitative analysis of these complicated processes in diamond is established. Furthermore, charge collection process in a diamond detector with incident protons is quantitatively studied by using this method. It can be concluded that the influence of carrier lifetime on charge collection efficiency (CCE) is saturated when the value of carrier lifetime is greater than the characteristic time for carriers to cover the diamond device. The influence of electric field on CCE is saturated when the value of electric field strength is greater than 1 MV/m. By comparison of the simulated results and the theoretical results of an ideal case, good agreements have been acquired in both saturated electric field and unsaturated electric field conditions. All these results indicate that this method is useful for quantitative simulation and further optimization design of diamond detectors and other devices.

Index Terms **—** Charge collection efficiency, charge collection mechanism, diamond, drift-diffusion model, semiconductor.

I. INTRODUCTION

Because of the distinguished material characteristics [1-4], including high response speed, low leakage current, high carrier drift velocity, excellent thermal hardness, and long carrier lifetime, the diamond material has attracted special attentions in high energy physics applications such as detectors of α particles [5], X-rays [6-8], neutrons [9, 10], and other devices [11-14].

Charge collection efficiency (CCE) plays a vital role in the performance of a particle detector. Many efforts have been taken on chemical vapor deposition and other experimental methods to ameliorate the CCE of the diamond detectors [5, 15]. Though quantitative analysis of the charge collection mechanism is important for the improvement of CCE, there is still a lack of effective methods to study this problem. Most of the actual case cannot be dealt with by theoretical analysis which is based on an ideal condition [15]. By the Monte Carlo (MC) method, the energy loss of incident particles in material can be derived [17], and the total amount of the electron/hole pairs (*e-h* pairs) ionized by the incident particle can also be derived. However, not all the *e-h* pairs can be collected. The carrier movement and the carrier recombination cannot be studied by the MC method directly, and the CCE cannot be derived. Because of the complexity of this multi-physics process, developing a quantitative method to analyze the charge collection mechanism of the diamond material remains difficult. To the best of authors' knowledge, very few researches have been reported about the multi-physics method that can be used to study the complex processes in the diamond.

In this study, a multi-physics method based on the drift-diffusion model (DDM) [16] is presented. The charge collection process of the diamond is analyzed by this method. Carrier generation, carrier movement, and carrier recombination are quantitatively researched. The influences of parameters of both the electric field and the diamond material on CCE are illustrated. This work provides an useful method for further optimization of diamond detectors and other devices. This is the main motivation of this work.

This paper is organized as follows. In Section II, the carrier ionizations inside the diamond caused by the incident particle and the carrier movements are expressed by Partial Differential Equations (PDEs). In Section III, a schematic structure of the diamond detector and its parameters are given. In Section IV, The carrier

Submitted On: December 26, 2018
Accepted On: April 3, 2019

1054-4887 © ACES

generation and carrier movement are presented. The influence of parameters of incident particles on CCE are illustrated in this section. The numerical results derived from this multi-physics method are theoretically verified. In Section V, some conclusions are given.

II. THEORETICAL MODEL

A. Mechanism of the diamond detector

Diamonds adopted in particle detectors are high-purity [1-3]. Without the incident particles, the free carriers are presented in the material due to thermal excitation. For intrinsic semiconductor material at finite temperature T, the intrinsic carrier concentration n_i can be expressed as follows [18, 19]:

$$n_i = \sqrt{N_C N_V}\exp(-\frac{E_g}{2k_b T}), \quad (1)$$

where N_c is the density of states on the bottom of the conduct band and N_v is the density of states on the top of the value band. The value of n_i can be derived by taking the material parameters in Table 1 into (1), and the intrinsic carrier concentration of the diamond at room temperature 300 K is 3.99×10^{-27} cm^{-3}. It is a very small value while the value of silicon material for Si-PIN detector is about 1.0×10^{10} cm^{-3} [18, 19]. However, because of unexpected impurities, a few carriers still exist in the diamond and can lead a leakage current without incident particles, which is usually less than 10×10^{-12} A [3, 15].

As illustrated in Fig. 1, when particles penetrate the diamond, *e-h* pairs are ionized along the tracks of particles. The electrons and holes are collected by the anode and the cathode respectively under a bias voltage and result in a current which can be measured in the back-end circuit.

In the rest parts of this section, the theoretical models of generation and movement of carries will be discussed in detail.

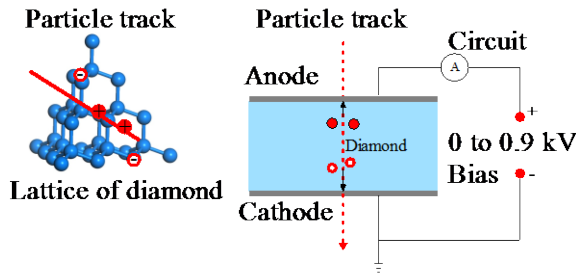

Fig. 1. The mechanism and the sketch map of the diamond detector. *e-h* pairs are ionized by incident particles in the diamond lattice. Then the *e-h* pairs are collected by electrodes under bias voltage results in a current, and the current can be detected by back-end circuit.

B. Equations of carrier ionization inside diamond

As analyzed in the previous part, without incident particles, the leakage current is very small. When particles penetrate into the diamond, the current in the diamond is much greater than the leakage current, and this current is mainly caused by the carriers ionized by incident particles. *e-h* pairs are ionized from the lattice of diamond by absorbing the energy lost by particles.

When a particle penetrates the diamond, the generation rate of *e-h* pairs induced by the particle can be expressed as a Gaussian function:

$$G_n = G_0 \exp[-\frac{(t-t_{\max})^2}{2\tau_0^{\ 2}}], \quad (2)$$

where t_{max} is the time instant when electron-hole pair generation rate reaches its maximum. τ_0 is the characteristic time. G_0 is the unitary constant which can be denoted as follows:

$$G_0 = \frac{2E}{E_0 \tau_0 \sqrt{\pi}}, \quad (3)$$

where E_0 is the average energy for generating a single *e-h* pairs, and the value is given in Table 1. E is the particle deposition energy, which is deposited by the carbon atoms of the diamond. The particle deposition energy in the diamond depends on the particle energy and particle species and can be numerically derived by the Monte Carlo simulation [17]. The particle deposition energy can be defined as:

$$E_{dep} = \int_0^{\lambda} \rho\delta(L)dL, \quad (4)$$

where δ is the linear energy transfer (LET) derived by the Monte Carlo simulation. ρ is the density of the diamond. λ is the incident depth of the particle.

The amount of *e-h* pairs of the unit length along the incident particle trace can be expressed as:

$$\Delta N = \frac{\rho\delta(L)}{E_0}. \quad (5)$$

The total amount of *e-h* pairs can be derived by the integral of (5) and can be expressed as:

$$N = \int_0^{\lambda} \frac{\rho\delta(L)}{E_0} dL = \frac{E_{dep}}{E_0}, \quad (6)$$

where the value of E_0 is given in Table 1.

C. Equations of carrier movement inside diamond

Behaviors of charges in electromagnetic field have attracted many attentions [20]. In this simulation, the DDM [16] has been used to describe the carrier movement inside other semiconductor material [21], and here is used to describe the diamond under a bias voltage, and can be expressed as follows:

$$\frac{\partial n_n}{\partial t} = \nabla\cdot(n_n\mu_n\mathbf{E} + \mu_n\frac{k_b T}{q}\nabla n_n) - (U-G), \quad (7)$$

$$\frac{\partial n_p}{\partial t} = -\nabla \cdot (n_p \mu_p \mathbf{E} - \mu_p \frac{k_b T}{q} \nabla n_p) - (U - G) , \qquad (8)$$

$$\nabla \cdot \varepsilon \nabla \psi = -q(n_p - n_p + N_D - N_A) - \rho_s , \qquad (9)$$

where n_n is the n-type carrier concentration and n_p for p-type, μ_n is the n-type carrier mobility and μ_p for p-type, **E** is the electric field, t is the time, T is the temperature, k_b is the Boltzmann constant, q is the unit charge, U is the recombination rate of carriers and G is the ionization rate. ε is the dielectric constant in the semiconductor. Ψ is the potential in the semiconductor. ρ_s is the surface charge density. N_D is the donor doping concentration and N_A is the acceptor doping concentration. For a high-purity diamond, N_D, ρ_s, and N_A are all set to be zero, then (9) can be written as:

$$\nabla \cdot \varepsilon \nabla \psi = -q(n_p - n_n) = \rho . \qquad (10)$$

In this study, n-type carriers are electrons ionized by incident particles, while p-type carriers are holes. T here is set to be uniform at room temperature 300 K.

Because of the high bias voltage which is attached to electrodes of the detector, the electric field inside the diamond is strong. The electron mobility and hole mobility in strong field can be expressed as:

$$\mu_i = \frac{\mu_{i0}}{1 + \mu_{i0} E / v_{si}} \ ,(\mathrm{i} = n, p) , \qquad (11)$$

where μ_{in} is the low field electron mobility. μ_{ip} is the low field hole mobility. μ_{sn} is the saturated velocity of electrons. μ_{sp} is the saturated velocity of holes. E is the electric field strength. The values are listed in Table 1.

D. Equations of carrier recombination inside diamond

When a bias voltage is applied to electrodes of the detector, carriers are moving toward electrodes, forced by electric field. However, not all of the carries can be collected by electrodes and come into current, a part of the *e-h* pairs recombine in the course moving towards electrodes. CCE η is defined as the ratio between collected charge and total generated charge and can be expressed as follows:

$$\eta = Q_c / Q_g . \qquad (12)$$

As a wide band gap semiconductor material, high-purity diamond analyzed here contains very few impurities, then the Shockley-Read-Hall (SRH) recombination which occurs nearby traps in energy gap is the primary mechanism of carrier recombination [18-19]. The SRH recombination rate U_{SRH} can be expressed as follows:

$$U_{\mathrm{SRH}} = \frac{n_p n_n - n_i^2}{\tau_p [n_n + n_i \exp(\frac{E_{trap}}{k_b T})] + \tau_n [n_p + n_i \exp(-\frac{E_{trap}}{k_b T})]} ,(13)$$

where τ_n is the n-type carrier lifetime and τ_p is the p-type carrier lifetime. E_{trap} is the energy difference between the trap energy level and the intrinsic Femi energy level. n_i is the intrinsic carrier concentration. n and p are respectively the n-type carrier concentration and the p-type carrier concentration.

III. NUMERICAL METHOD

Finite element method and Finite Volume Method (FVM) are used to carried out the PDEs of electromagnetic problems [22-23] and the DDM [24-25]. In this paper, FVM is adopted. In order to describe the DDM briefly, solution vector **Q**, flux vector **F**, and source term **S** are introduced into the equations, they can be expressed as follows:

$$\mathbf{Q} = \begin{pmatrix} 0 \\ n_n \\ n_p \end{pmatrix} , \qquad (14)$$

$$\mathbf{F} = \begin{pmatrix} \varepsilon \nabla \psi \\ \frac{1}{q} \mathbf{J}_n \\ -\frac{1}{q} \mathbf{J}_p \end{pmatrix} , \qquad (15)$$

$$\mathbf{S} = \begin{pmatrix} \rho \\ U - G \\ U - G \end{pmatrix} . \qquad (16)$$

where the current density vectors **J** is defined as:

$$\mathbf{J} = \mathbf{J}_n + \mathbf{J}_p , \qquad (17)$$

where electron current density vectors and hole current density vectors are defined as:

$$\mathbf{J}_n = n_n \mu_n \mathbf{E} + \mu_n \frac{k_b T}{q} \nabla n_n , \qquad (18)$$

$$\mathbf{J}_p = n_p \mu_p \mathbf{E} + \mu_p \frac{k_p T}{q} \nabla n_p . \qquad (19)$$

Equations of the DDM can be expressed as:

$$\frac{\partial \mathbf{Q}}{\partial t} = \nabla \cdot \mathbf{F} + \mathbf{S} . \qquad (20)$$

Using the Green's equation, it can be expressed as:

$$\int_{\Omega_m} \frac{\partial \mathbf{Q}_m}{\partial t} dV = \sum_e \mathbf{F}_e l_e + \int_{\Omega_i} \mathbf{S}_m dV \mathbf{S} , \qquad (21)$$

where Ω_m is the m controlled volume, $\mathbf{F}_{\mathrm{e}}$ is the projection component of **F** in the boundary of controlled volume. l_e is length of the boundary.

Electron and hole concentrations in a controlled volume are both set to be uniform approximately. Then the left side of Eq. (21) can be expressed as:

$$\int_{\Omega_m} \frac{\partial \mathbf{Q}_m}{\partial t} dV = \frac{\partial \mathbf{Q}_m}{\partial t} \Delta V_{\Omega_m} , \qquad (22)$$

where $\Delta V_{\Omega m}$ is the cubage of controlled volume m.

The generation of carrier is set to be as initial condition before the calculation, and the generation of carrier during a single time step is ignored. Meanwhile, the recombination rate is set to be constant. Then the source term **S** can be expressed as:

$$\int_{\Omega_m} \mathbf{S}_m dV = \mathbf{S}_m \Delta V_{\Omega_m} . \qquad (23)$$

In the calculation, triangle mesh of controlled volume as shown in Fig. 2 are adopted. Then the functions of flux in points i, j and k can be expressed as:

$$\mathbf{F}_i = (J_j d_j - J_k d_k)\hat{n}, \quad (24)$$

$$\mathbf{F}_j = (J_k d_k - J_i d_i)\hat{n}, \quad (25)$$

$$\mathbf{F}_k = (J_i d_i - J_j d_j)\hat{n}, \quad (26)$$

where i, j, and k are the vertexes of the triangle mesh of controlled volume m respectively. $\hat{n}$ is the unit vector along the direction of the flux. Point O is the center of circumcircle of the triangle mesh. $\widehat{s_i}$, $\widehat{s_j}$, and $\widehat{s_k}$ are the unit vectors in boundaries of a triangle mesh respectively. J_i, J_j, and J_k are the average projections of current in the boundaries of i, j and k of the triangle mesh respectively. J_k can be expressed as:

$$J_k = \mathbf{J} \cdot \widehat{s_k}. \quad (27)$$

In the calculation, electric field strength and current vary slowly along the boundary of the triangle mesh, then this problem can be dealt as three one-dimension problems. Then electron current and hole current of J_k in (27) can be expressed respectively as follows:

$$J_{nk} = \frac{q\mu_n V_T}{L_k}[n_{nj}B(\frac{\psi_j - \psi_j}{V_T}) - n_{ni}B(-\frac{\psi_j - \psi_i}{V_T})], \quad (28)$$

$$J_{pk} = \frac{q\mu_p V_T}{L_k}[n_{pi}B(\frac{\psi_j - \psi_j}{V_T}) - n_{pj}B(-\frac{\psi_j - \psi_i}{V_T})], \quad (29)$$

where V_T is the threshold voltage of the diamond material, defined as:

$$V_T = \frac{k_b T}{q}. \quad (30)$$

Function B in (28) and (29) is the Bernoulle function, and can be expressed as:

$$B(x) = \frac{x}{e^x - 1}. \quad (31)$$

J_i and J_j can be derived by the same steps. The steps of the calculation are shown in the flowchart of Fig. 3.

IV. PARAMETERS OF THE DIAMOND DETECTOR

The working mechanism of the diamond detector is briefly described in part II. In this simulation, the diamond detector is set to be cylindrical symmetry as illustrated in Fig. 1. A finite volume method code as introduced in Section III is used to carry out the PDEs. The material parameters of the diamond used in the simulation are shown in Table 1. The thickness of the diamond in the detector is set to be 300 μm as reported [15].

The generation of carriers follows a Gaussian function as denoted in (2). In the following numerical simulations, t_{max} is set to be 10 ps and characteristic time τ_0 is set to be 1 ps.

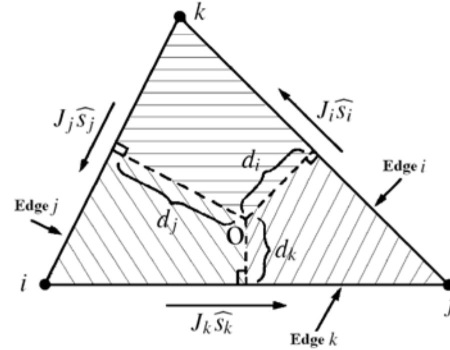

Fig. 2. The triangle mesh in the code.

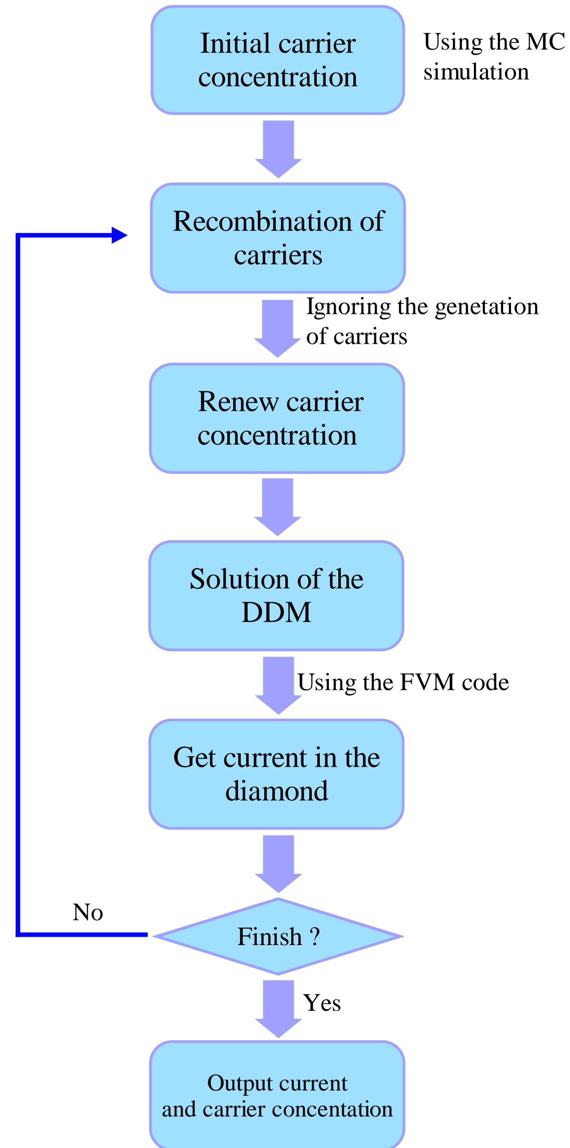

Fig. 3. Flowchart of the simulation.

Table 1: Material parameters of the diamond used in the simulation

Parameters	Parameter Name	Value
E_g	Band gap of diamond	5.5 eV
T_m	Melting point	4273 K
E_{Af}	Affinity of Si	4.15 eV
ε_{dia}	Relative permittivity of the diamond	5.7
μ_{n0}	Low field electron mobility	1714 cm^2/V/s
μ_{p0}	Low field hole mobility	2064 cm^2/V/s
v_{sn}	Electron saturated velocity	9.6×10^6 cm/s
v_{sp}	Hole saturated velocity	14.1×10^6 cm/s
N_c	Density of states on bottom of conduct band	6.57×10^{19} cm^{-3}
N_v	Density of states on top of value band	1.80×10^{19} cm^{-3}
E_0	Ionization energy of a single *e-h* pair	13 eV
E_{BR}	Breakdown field	10×10^4 V/cm
ρ (dia)	Density of diamond	3.515 g/cm^{-3}
c_p (dia)	Specific heat of diamond	0.52 J/g/K
k_b	Boltzmann constant	1.381×10^{-23} J/K
q	Unit charge	1.602×10^{-19} C

The LET depends on parameters of the incident particles. In the simulation, incident particles are all protons, so the energy of the incident proton is the dominant of the LET. Four proton energies are studied in the simulation, they are 4.5 MeV, 6.62 MeV, 7.65 MeV, and 9.71 MeV. In the following simulations, LET of different protons is set according to the MC simulation results which are illustrated in Table 2. As shown in Fig. 4, the 9.71 MeV proton penetrates through the diamond, other three are absorbed by the diamond. The density of *e-h* pairs along the trace of the incident proton can be derived by (6).

The Bias voltage is set from 50 V to 900 V. So the electric field in the diamond varies from 0.6×10^6 V/m to 3×10^6 V/m, and is less than the breakdown field as listed in Table 1.

The interfaces between the diamond and metal electrodes are set to be Ohmic contact boundaries.

By using the parameters in Table 1, the electron velocity and the hole velocity can be derived from (11) as illustrated in Fig. 5. When the electric field is greater than 1×10^6 V/m, both the electron velocity and the hole velocity increase very slowly versus the electric field strength and reach saturation points gradually.

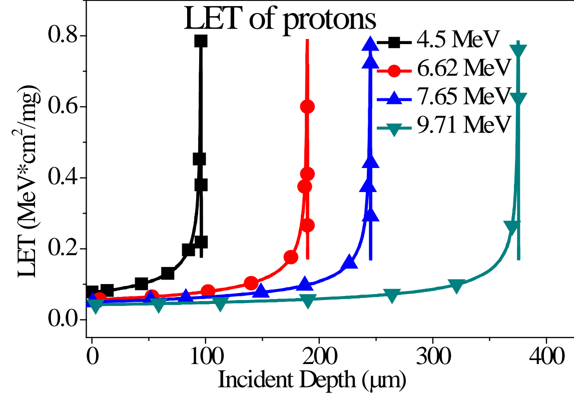

Fig. 4. The values of LET derived by the MC simulation. The proton energies are 4.5 MeV, 6.62 MeV, 7.65 MeV and 9.71 MeV. The 9.71 MeV proton penetrates through the diamond.

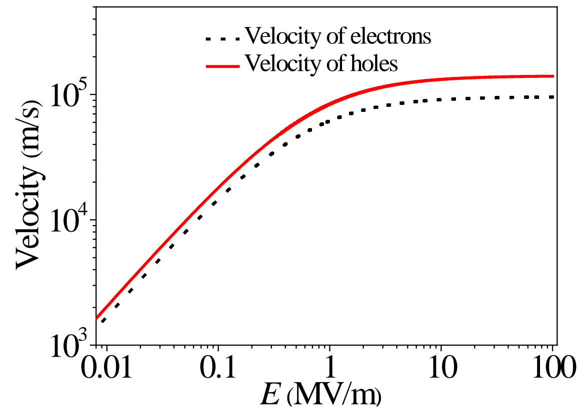

Fig. 5. Velocity of electrons and holes vs. electric field based on (11).

Table 2: Mc simulation results of the protons

Energy of Proton	Incidence Depth	Ionized Charge
4.5 MeV	96.19 μm	5.496×10^{-14} C
6.62 MeV	189.87 μm	8.073×10^{-14} C
7.65 MeV	245.32 μm	9.934×10^{-14} C
9.71 MeV	300 μm	7.096×10^{-14} C

V. CALCULATION RESULTS AND DISCUSSION

The initial distributions of space charges which are generated by the 4.5 MeV proton and the 9.71 MeV proton are illustrated in Fig. 6. The values of LET in the end of the incident traces are much higher, so the amount of charges in these positions are much higher. On the contrary, the 9.71 MeV proton penetrates through the

diamond, and the charge concentration is uniform because of the uniform LET. Electric fields of both two cases are affected by the distribution of space charges, as illustrated in Fig. 6.

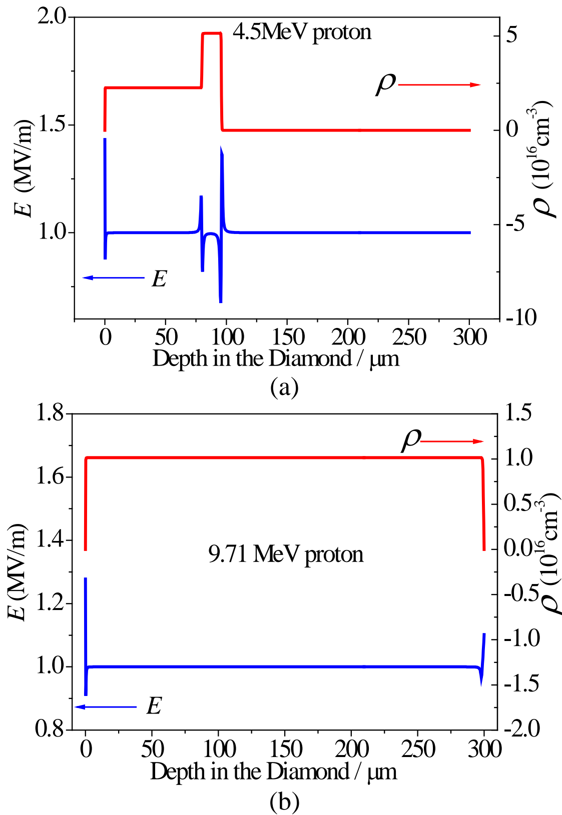

Fig. 6. The initial concentration of the space charges ionized by the proton. Energies of incident protons are 4.5 MeV and 9.71 MeV respectively. The lifetime of carriers is 1 ns. The electric field in the diamond is 1 MV/m. (a) 4.5 MeV and (b) 9.71 MeV.

The currents in the electrodes, which are induced by different incident protons are illustrated in Fig. 7. Every current in Fig. 7 consists of two parts: the displace current part and the conduction current part. The displace current part arises at almost the same time when space charges are generated by the incident protons. The conduction current part arises later, limited by the velocities of electrons and holes.

The peak value of the displace current part is determined by the total amount of the space charges, and the peak value is not affected by the carrier lifetime, as illustrated in Fig. 8. However, the conduction current part is determined by the amount of charges which are collected by the electrodes. Shorter carrier's lifetime means higher probability of charge recombination, which results in a greater loss of the charges which can arrive in electrodes. The currents of different carrier lifetimes are illustrated in Fig. 8.

More details of the charge collection mechanism and the movements of charges will be discussed in the following parts.

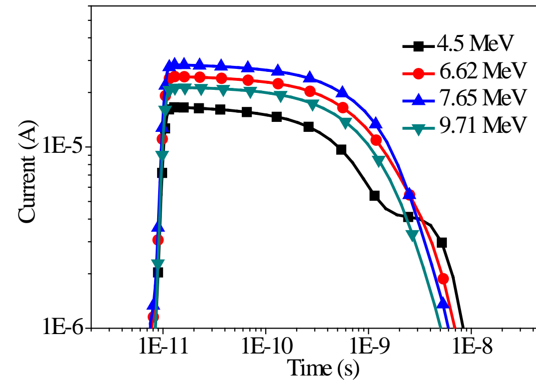

Fig. 7. Currents in the diamond. Energies of incident protons are 4.5 MeV, 6.62 MeV, 7.65 MeV and 9.71 MeV respectively. The lifetimes of the carriers are all 1 ns. The electric field in the diamond is 1 MV/m.

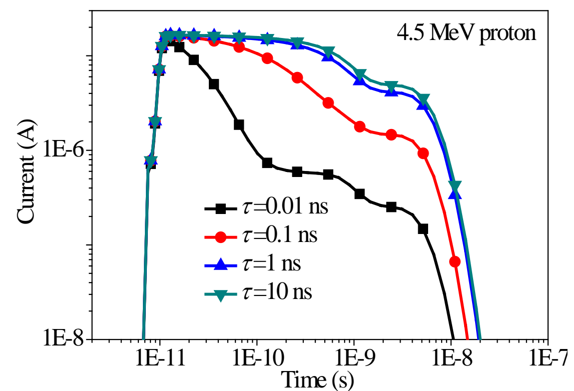

Fig. 8. Currents in the diamond. Energy of the incident proton is 4.5 MeV. The carrier lifetimes are 0.01ns, 0.1 ns, 1 ns and 10 ns, respectively. The electric field in the diamond is 1 MV/m.

A. Movements of charges

The charge concentrations at different time are illustrated in Fig. 9. Because of the carrier recombination, the peak value of charge concentrations falls down at the later time. Simultaneously, the space charges move towards the electrodes forced by the electric field.

B. Influence of the carrier lifetime

As mentioned in Fig. 8, shorter carriers lifetime results in a greater loss of the charges which can arrive in electrodes. The distributions of electrons and holes with various carrier lifetimes are illustrated in Fig. 10. During the same time, carriers of shorter lifetime recombines at a higher probability, result in a smaller peak value of

concentration.

The flight time for carriers to cover the diamond can be derived as:

$$\Delta t = L / (v_n + v_p), \qquad (32)$$

where L is the distance between the cathode and the anode. v_n is the electron velocity and v_p is the hole velocity. When the electric field in the diamond is 1 MV/m, v_n = 6.1573×10^4 m/s, v_n =8.3772×10^4 m/s. Then Δt = 2.07 ns. If the values are greater than Δt, the influence of carrier lifetime on increasing CCE becomes exiguous. The results are illustrated in Fig. 11.

C. Influence of electric field

The drift velocity of electrons and holes versus electric field is expressed in (11) and illustrated in Fig. 5. The drift velocity becomes saturated when the electric field is greater than 1 MV/m. As illustrated in Fig. 12, the influence of electric field on the movements of carriers becomes exiguous when the electric field is greater than 1 MV/m. The influence of the electric field on CCE is illustrated in Fig. 13. For all the four incident protons, the saturated values of CCE are derived when the electric field is greater than 1 MV/m.

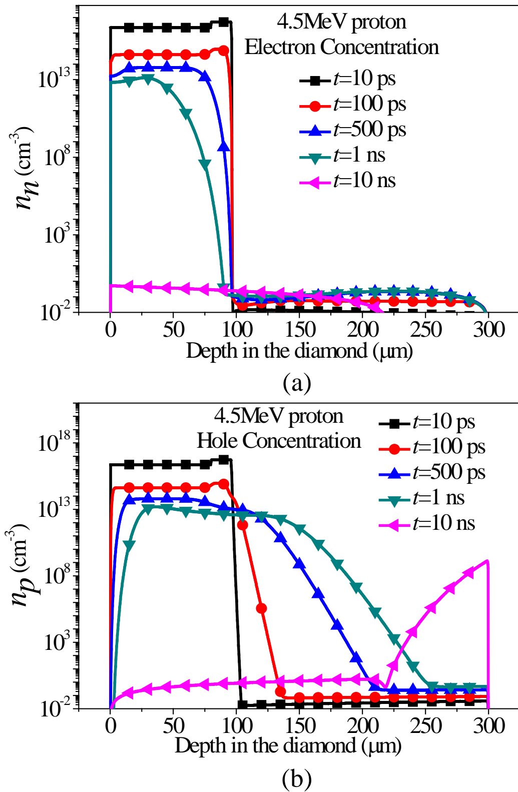

Fig. 9. The charge concentrations at different time. The energy of the incident particle is 4.5 MeV. The lifetimes of carriers are 1 ns. The electric field in the diamond is 1 MV/m: (a) the electron concentrations and (b) the hole concentrations.

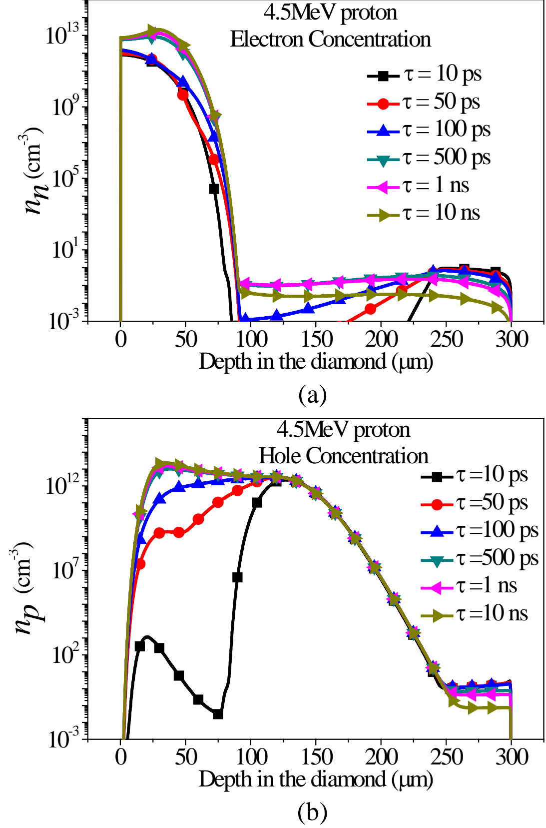

Fig. 10. The charge concentrations with various carrier lifetimes. The energy of the incident particle is 4.5 MeV. The electric field in the diamond is 1 MV/m. The time is 1 ns after the proton penetrated into the diamond: (a) the electron concentrations and (b) the hole concentrations.

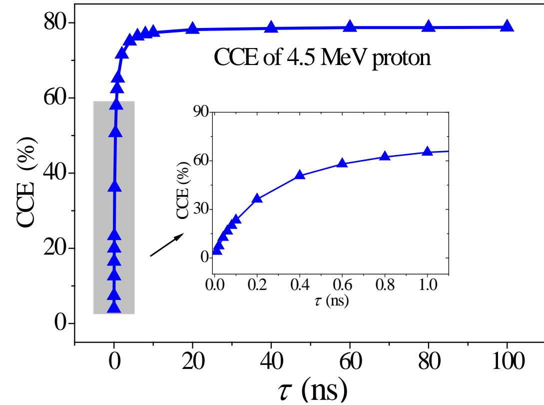

Fig. 11. CCE of the diamond with various lifetimes of carriers. The energy of the incident particle is 4.5 MeV. The electric field in the diamond is 1 MV/m.

D. Verification of the method

In the case of a perfect and uniform distribution of space charges, the CCE can be theoretically derived [15, 26], and can be written as a function of charge collection

distance (CCD) as:

$$\eta = \frac{\sigma}{L}[1 - \frac{\sigma}{4\lambda}(1 - e^{-2\lambda/\sigma})(1 + e^{2(\lambda - L)/\sigma})]. \quad (33)$$

where L is the distance between cathode and anode. λ is the incident depth of radiation particles. In the penetrating-through case, λ is set to be equal to L. The CCD is defined as:

$$\sigma = (\frac{\mu_n}{1 + \mu_n E / v_{sn}} + \frac{\mu_p}{1 + \mu_p E / v_{sp}})\tau E = (v_n + v_p)\tau. \quad (34)$$

where v_n is the electron velocity and v_p is the hole velocity, as mentioned in (11). τ is the average carrier lifetime. The values of τ are reported to be in a range of 10^2~10^3 ps [15] to 30 ns [27].

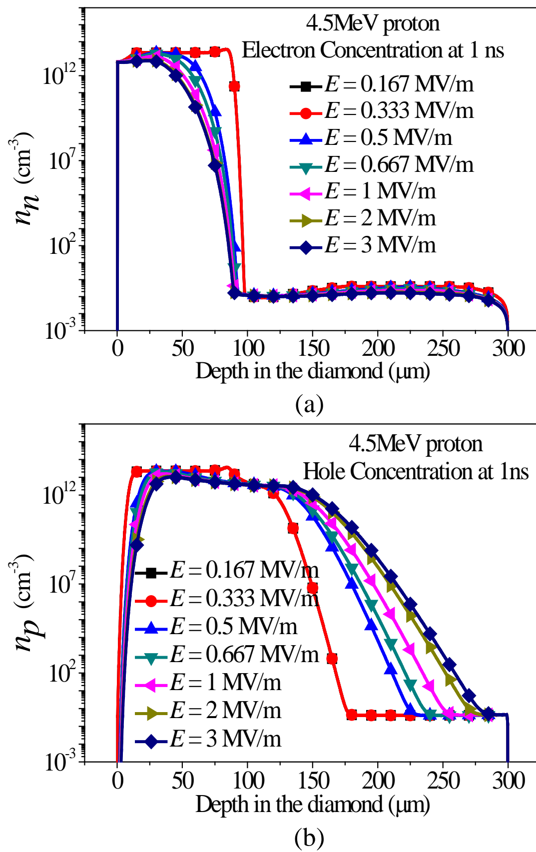

Fig. 12. The charge concentrations with various electric fields. The energy of the incident particle is 4.5 MeV. The lifetime of carriers is 1 ns: (a) the electron concentrations and (b) the hole concentrations.

The theoretical results derived from (34) is based on the physical hypothesis: carriers, both electrons and holes, distribute uniformly in the whole the diamond. However, as shown in Fig. 6, this ideal hypothesis is hard to achieve in a real case. Carrier concentrations in the case of 9.71 MeV proton can be treated as uniform approximately as shown in Fig. 6. Comparisons of simulated results based on this multi-physics method and theoretical results from (33) are illustrated in Fig. 14. In the case of small CCE, which means the length of the trace for a single carrier is short, the heterogeneity during the trace is also small and can be ignored. In that case, the difference between the simulated results and the results from (33) is small. In the case of large CCE, which means the length of the trace for a single carrier is great, the heterogeneity during the trace becomes great. As a result, the difference between simulated results and the results from (33) becomes great.

As shown in Fig. 14, curves in small CCE case and large CCE case both follow the analysis mentioned above. This result indicates that this multi-physics method is physically reliable. Meanwhile, this method is effective for the complicated case which does not match the ideal hypothesis.

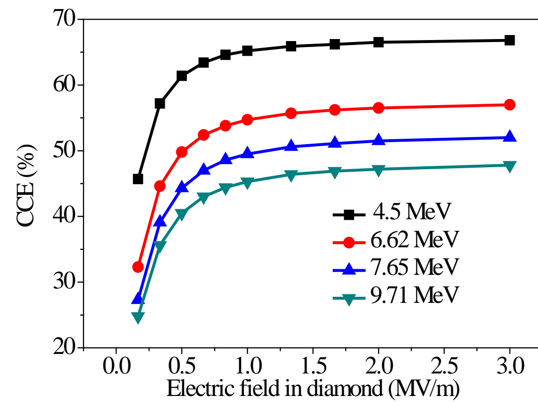

Fig. 13. CCE of the diamond versus electric field. Energies of the incident protons are 4.5 MeV, 6.62 MeV, 7.65 MeV and 9.71 MeV respectively. The lifetimes of the carriers are all 1 ns.

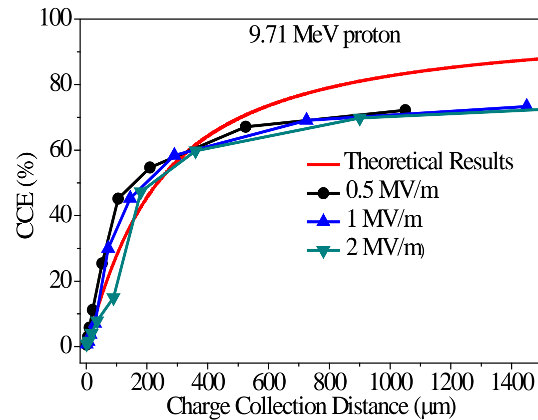

Fig. 14. CCE comparisons between the simulated results and the theoretical results based on (33).

VI. SUMMARY AND CONCLUSION

In this paper, a multi-physics method which synthesizes the complicated processes of the diamond is presented. The carrier generation, carrier recombination and carrier movement are analyzed quantitatively by this method. Based on the previous analyses, conclusions are made as follows:

1) The current in the diamond induced by an incident proton consists of two parts: the displace current part and the conduction current part. The peak value of the displace current part is determined by the total amount of space charges which are generated by the incident protons.

2) The carrier lifetime and the electric field are important factors of CCE. The influence of carrier lifetime is saturated when the value of carrier lifetime is greater than the flight time for carriers to cover the diamond. The influence of electric field is saturated when the value of electric field strength is greater than 1 MV/m.

3) This multi-physics method is verified by the comparison between the simulated results using this method and the theoretical results. Good agreements are presented in both saturated electric field and unsaturated electric field.

This work brings an effective method for quantitative analysis of diamond detectors and is useful for further optimization of diamond detectors and other diamond devices.

ACKNOWLEDGMENT

This work was supported by the National Natural Science Foundation of China (under Grant 61231003 and Grant 11605140).

The authors would like to thank Prof. Xiaoping Ouyang of the Northwest Institute of Nuclear Technology for the discussion on the interaction between particles and the diamond.

Also thank Dr. Chen Shen and Ding Gong of the Cogenda Company for their helps on the MC simulation.

REFERENCES

[1] J. Isberg, J. Hammersberg, E. Johansson, et al., "High carrier mobility in single-crystal plasma-deposited diamond," *Science*, vol. 297, pp. 1670-1672, 2002.

[2] H. Kagan, "Recent advances in diamond detector development," *Nucl. Instr. and Meth. A*, vol. 541, pp. 221-227, 2005.

[3] X. Ouyang, L. Wang, R. Fan, et al., "Preparation of diamond film based radiation detector," *Acta. Phys. Sin.*, vol. 55, no. 5, pp. 2170-2174, 2006.

[4] S. Almaviva, M. Marinelli, E. Milani, et al., "Chemical vapor deposition diamond based multi-layered radiation detector: Physical analysis of detection properties," *Journal of Applied Physics*, vol. 107, no. 1, p. 014511, 2010.

[5] M. Marinelli, E. Milani, A. Paoletti, et al., "High-quality diamond grown by chemical-vapor deposition: Improved collection efficiency in α-particle detection," *Applied Physics Letters*, vol. 75, no. 20, pp. 3216-3218, 1999.

[6] L. Hou, F. Li, Y. Yuan, et al., "Chemical vapor deposited diamond detectors for soft X-ray power measurement," *Acta. Phys. Sin.*, vol. 59, no. 02, pp. 1137-1141, 2010.

[7] B. Yu, B. Chen, L. Hou, et al., "Hard X-ray measurement for indirect-driven imploding by chemical vapor deposited diamond detectors," *Acta. Phys. Sin.*, vol. 62, no. 5, p. 058102, 2013.

[8] L. Liu, X. Ouyang, J. Zhang, et al., "Properties comparison between nanosecond X-ray detectors of Polycrystalline and single-crystal diamond," *Diamond & Related Materials*, vol. 73, pp. 248-252, 2017.

[9] M. Marinelli, E. Milani, G. Prestopino, et al., "High performance ^{6}LiF-diamond thermal neutron detectors," *Applied Physics Letters*, vol. 297, no. 14, p. 143509, 2002.

[10] L. Liu, X. Ouyang, Z. Zhang, et al., "Polycrystalline chemical-vapor-deposited diamond for fast and ultra-fast neutron detector," *Science China: Technological Sciences*, vol. 22, no. 9, pp. 2640-2645, 2012.

[11] X. Chang, Q. Wu, I. Ben-Zvi, et al., "Electron beam emission from a diamond-amplifier cathode," *Physics Review Letters*, vol. 105, no. 16, p. 164801, 2010.

[12] L. Liu, X. Ouyang, J. Zhang, et al., "Polycrystalline diamond based detector for Z-pinich plasma diagnosis," *Review of Scientific Instruments*, vol. 81, no. 8, p. 083502, 2010.

[13] L. Liu, X. Ouyang, J. Zhang, et al., "Polycrystalline CVD diamond detector: Fast response and high sensitivity with large area," *AIP Advanced*, vol. 4, no. 1, pp. 017114, 2014.

[14] X. Wang, J. Wang, and L. Wang, "Single-layer nano-carbon film, diamond film, and diamond/ nano-carbon composite film field emission performance comparison," *Applied Physics Letters*, vol. 108, no. 19, p. 191602, 2016.

[15] L. Wang, "Studies on CVD Diamond Detectors for Pulsed Radiation Detection," *Ph.D. Thesis*, Tsinghua University, Beijing, China, 2008.

[16] H. K. Gummel, "A self-consistent iterative scheme for one-dimensional steady state transistor calculations," *IEEE Trans. Electron Devices*, vol. 9, no. 11, pp. 455-465, 1964.

[17] S. Agostinelli, J. Alison, K. Amoko, and et al., "GEANT4: A simulation toolkit," *Nucl. Instr. and Meth. A*, vol. 506, pp. 250-303, 2003.

[18] S. M. Sze and K. K. Ng, *Physics of Semiconductor*

Devices. 3rd edition, New York: John Wiley & Sons, 2006.

[19] L. Ye, *Physics of Semiconductor*. Beijing, China: Beijing, Higher Education Press, 2007.

[20] J. Wang, D. Zhang, C. Liu, et al., "UNIPIC code for simulation of high power microwave devices," *Physics of Plasma.*, vol. 16, no. 3, pp. 03310801-03310810, 2009.

[21] H. Bao, D. Ding, J. Bi, W. Gu, and R. Chen, "An efficient spectral element method for semiconductor transient simulation," *Applied Computational Electromagnetics Society Journal*, vol. 31, no. 11, pp. 1337-1342, 2016.

[22] Y. Zhou, L. Shi, N. Liu, C. Zhu, H. Liu, and Q. H. Liu, "Spectral element method and domain decomposition for low frequency subsurface," *IEEE Geosci. Remote Sens. Lett.*, vol. 13, no. 4, pp. 550-554, 2016.

[23] Y. Zhou, L. Shi, N. Liu, C. Zhu, Y. Sun, and Q. H. Liu, "Mixed spectral-element method for overcoming the low-frequency breakdown problem in subsurface EM exploration," *IEEE Geosci. Remote Sens.*, vol. 55, no. 6, pp. 3488-3500, 2017.

[24] A. Jameson, "A solution of the Euler equations for two dimensional transonic flow by a multi-grid method," *Applied Mathematics and Computation.*, vol. 13, pp. 327-355, 1983.

[25] J. V. Soulis, "Finite volume method for three-dimensional transonic potential flow through turbo-machinery blade rows," *International Journal of Heat and Fluid Flow.*, vol. 4, no. 2, pp. 85-96, 1983.

[26] K. Hecht, "Zum mechanismus des lichtelektrischen primarstromes in isolierenden kristallen," *Z. Physik*, vol. 77, pp. 235-245, 1932.

[27] H. Pernegger, S. Roe, P. Weilhammer, et al., "Charge-carrier properties in synthetic single-crystal diamond measured with the transient-current technique," *Journal of Applied Physics*, vol. 97, no. 07, p. 073704, 2005.

Yong Li was born in Anhui Province, P.R. China, on January 28, 1984. He obtained the B.S. and M.S. degrees in Physics from University of Science and Technology of China (USTC), Hefei Anhui, P.R. China, in 2006 and 2009 respectively. Since 2016, he is currently working toward the Ph.D. degree in the School of Electronic and Information Engineering, Xi'an Jiaotong University, Xi'an, P.R. China.

He is currently with the Northwest Institute of Nuclear Technology (NINT) as an Assistant Scientist. His research interests mainly include electromagnetic compatibility, electromagnetic effect of semiconductor devices and circuits.

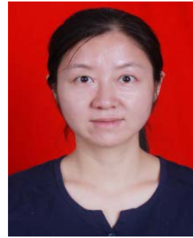

Haiyan Xie was born in Anhui Province, P.R. China, on February 27, 1984. She received the B.S. and Ph.D degrees in Engineering Physics from Tsinghua University, Beijing, P.R. China, in 2005 and 2010, respectively. She received best doctoral thesis of Tsinghua University in 2010.

During 2011 to 2012, she conducted her post-doctoral research at Northwest Institute of Nuclear Technology (NINT). Now, she serves NINT as an associate scientist.

Her research interests mainly include electromagnetic compatibility, electromagnetic interference, and transmission line analysis.

Linyue Liu was born in Shannxi Province, P.R. China, 1983. She obtained the B.S. degree in Material Physics from University of Science and Technology of China (USTC), Hefei Anhui, P.R. China, in 2005. She obtained the Ph.D. degree in Nuclear Science and Technology from Xi'an Jiaotong University, Xi'an, P.R. China in 2018.

Her research interests mainly include neutron detection, wide-gap semiconductor detectors, and particle physics.

Jianfu Zhang was born in Jiangxi Province, P.R. China, 1977. Now, he serves NINT as an Associate Scientist. His research interests mainly include detectors and particle physics.